Electronic Supplementary Material (ESI) for Chemical Science.

Supporting Information

Confined Space Synthesis of Nanostructured Anatase Directed by Genetically Engineered Living Organism for Lithium-ion Batteries

Hang Ping, Hao Xie, Mingyu Xiang, Bao-Lian Su, Yucheng Wang, Jinyong Zhang, Fan Zhang, and Zhengyi Fu**

Experimental Section

Construction and Expression of Recombinant Proteins: The coding sequence of ice nucleation protein (INP) and selected regions of silaffin protein (5R5) was synthesized and cloned into a pET28a(+) vector (Novagen, Germany). The resultant plasmid is pET(INP-5R5), encoding the gene of protein INP-5R5 (Fig. S3†). The plasmid of pET(INP-nR5) (n=1, 3) was obtained from pET(INP-5R5) through inverse polymerase chain reaction. All constructs were confirmed by DNA sequencing. The expression procedure of INP-nR5 (n=1, 3, 5) was based on pET System Manual (Novagen, Germany). A single colony of *E. coli* BL21(DE3) harboring pET(INP-nR5) was inoculated into Luria-Bertani (LB) medium containing 30 μg mL^{-1} Kanamycin with continuous shaking at 37 °C overnight. The cell suspension was inoculated into LB medium, followed by shaking at 37 °C until an optical density (OD_{600}) of 0.5-0.6 was reached. Protein expression was initiated by a supply of 1.0 mM isopropyl-p-D-thiogalactoside (IPTG) and shaking at 30 °C for 3 hours. Cells were harvested by centrifugation at 8,000 g and 4 °C, re-suspended into buffer A (50 mM Tris-HCl, pH 8.5; 100 mM NaCl), and then lysised through a French press at 14 MPa. The cell lysate was centrifuged at 5,000 g for 10 min, and the supernatant was then centrifuged at 12,000 g for 50 min to collect cell membrane debris. The total proteins of induced cells and cell membrane debris were analyzed by sodium dodecyl sulfate polyacrylamide gel electrophoresis (SDS-PAGE).

Preparation of nanostructured anatase: *E. coli* cell pellets were re-suspended in 10 mL TBS buffer (50 mM Tris-HCl, pH 7.0, 300 mM NaCl), followed by dropwise addition of 2 mL titanium (IV) bis(ammonium lactato) dihydroxide solution (TiBALDH, Sigma-Aldrich, USA). The reaction mixture was incubated at 37 °C with gentle shaking for 24 hours and then transferred into water bath at 80 °C for 24 hours to allow mineralization. The products were isolated by centrifugation and washed with deionized water, then dried in a lyophilizer. Finally, the products were annealed in a muffle furnace and tubular furnace at 600 °C for 4 hours at a heating rate of 10 °C min^{-1} in air and 4 °C min^{-1} in Ar, respectively. The products were embedded in epoxy resin at 37 °C, then ultrathin sections were prepared by ultramicrotome in Leico EMUC7.

Characterization of nanostructured anatase: X-ray diffraction (XRD) patterns were performed using Bruker D8 Advance with Cu Kα radiation (V = 40 kV, I = 40 mA) in the range of 20-80°. Surface morphology information was revealed by field emission scanning electron microscopy (FESEM) in a Hitachi S-4800 at 5 kV equipped with an energy-dispersive spectroscopy (EDS) detector. High resolution transmission electron microscopy (HRTEM) examination was carried out with a JEOL JEM 2100F at 200 kV. Specific surface area was determined in an ASAP 2020M adsorption apparatus using the Brunauer-Emmet-Teller (BET) method. The Raman spectrum was obtained in a Renishaw InVia Raman spectrometer with excitation by Nd: YAG laser operating at 785 nm. Thermogravimetric (TG) analysis was performed in a Netzsch STA449F3 at a heating rate of 10 °C min^{-1} from 40 °C to 900 °C.

Electrochemical Measurements: Electrochemical performance of the electrode was carried out in a CR2025-type coin cells with lithium metal foil as the counter and reference electrodes. To fabricate the working electrode, a N-methyl-2-pyrrolidone (NMP, Aladdin, China) slurry of active materials was mixed with Super P carbon black and polyvinylidene fluoride in a weight ratio of 7:2:1. After intensive grinding, the resultant slurry was pasted on Cu foil and vacuum dried at 120 °C for 12 hours. The mass loading was about 1.5 mg active materials each coin cell. Coin cells were assembled in an Ar-filled glove box, and 1 M lithium hexafluoro-phosphate in ethylene carbonate (EC)/diethyl carbonate (DEC) (1:1 v/v) was used as the electrolyte solution. Celgard polypropylene was used as the separator. The charge-discharge experiments were carried on using a LAND battery tester CT2001A with a voltage window of 1-3 V (vs Li^+/Li) at various current densities (1 C = 167 mA g^{-1}). The electrochemical impedance spectroscopy (EIS) analysis was conducted using Autolab PGSTAT 302N equipment with the frequency range from 100 kHz to 0.01 Hz. Cyclic voltammetric (CV) test was performed in an electrochemical workstation with 1-3 V (vs Li^+/Li) at different scanning rates.

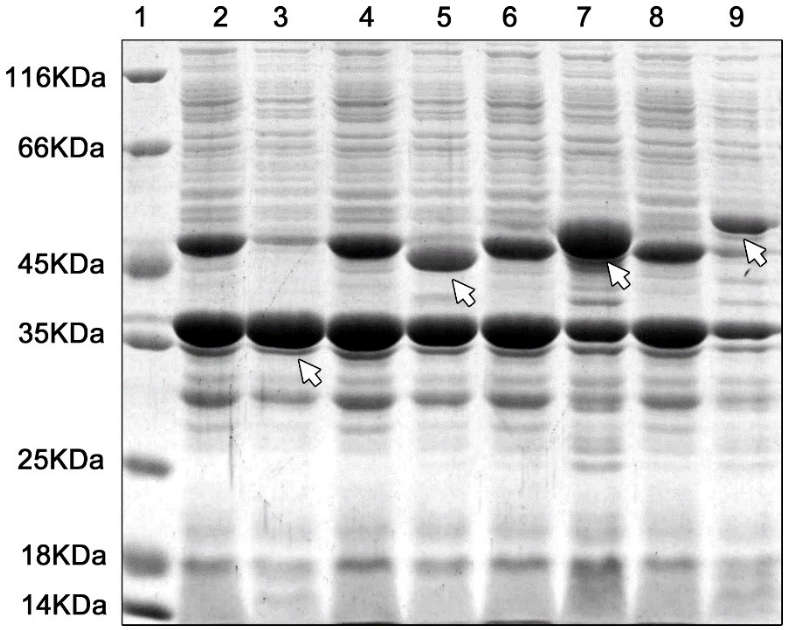

Fig. S1 Membrane protein gel electrophoresis of INP-nR5 (n=1, 3, 5) and INP, analyzed with 10% SDS-PAGE. (a) Lane 1, molecular weight marker; lanes 2 and 3, un-induced cells and IPTG-induced INP cells, respectively; lanes 4 and 5, un-induced cells and IPTG-induced INP-R5 cells, respectively; lanes 6 and 7, un-induced cells and IPTG-induced INP-3R5 cells, respectively; lanes 8 and 9, un-induced cells and IPTG-induced INP-5R5 cells, respectively. The target bands were marked by arrows.

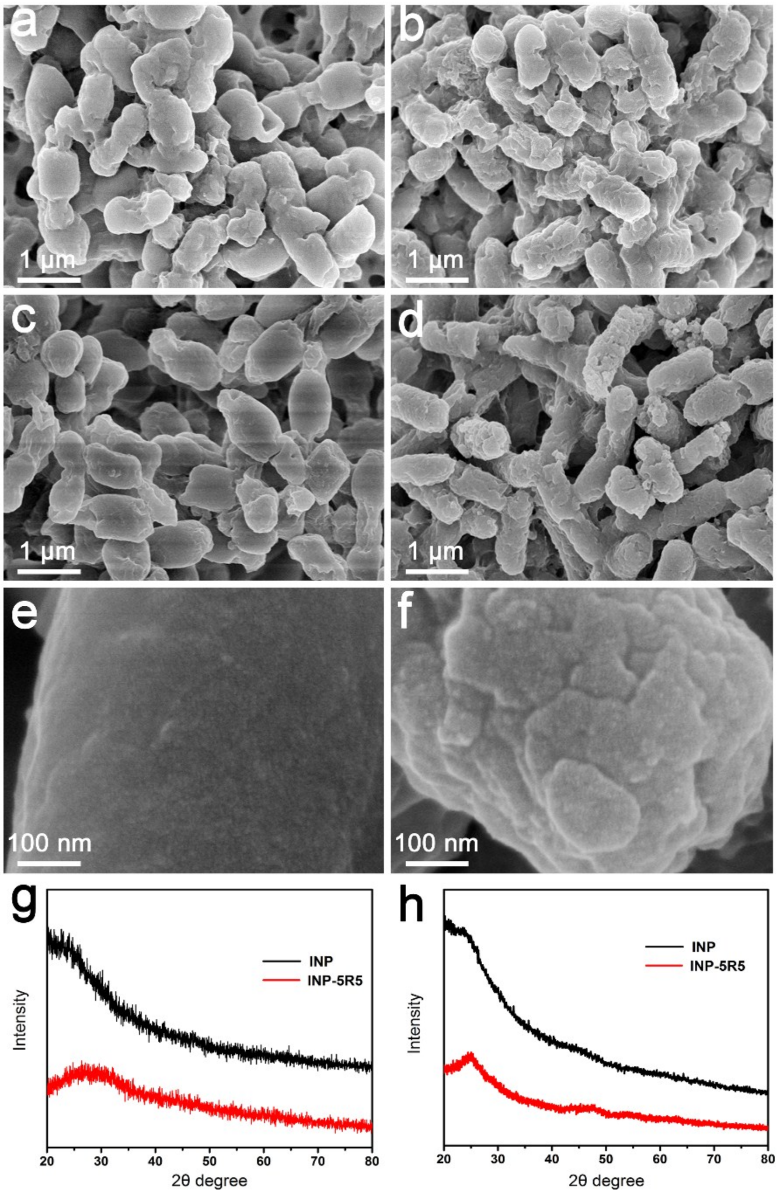

Fig. S2 Mineralization of genetically engineered bacteria. SEM images of (a) INP and (b) INP-5R5 modified cells after incubation at 37 °C for 24 hours. SEM images of (c) (e) INP and (d) (f) INP-5R5 modified cells after continuous incubation at 37 °C and 80 °C for 24 hours. XRD pattern of INP modified and INP-5R5 modified products after (g) incubation at 37 °C for 24 hours, (h) continuous incubation at 37 °C and 80 °C for 24 hours.

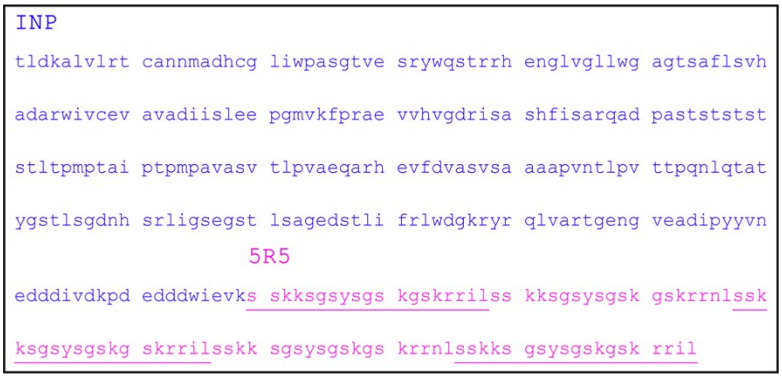

INP

tldkalvlrt cannmadhcg liwpasgtve srywqstrrh englvgllwg agtsaflsvh

adarwivcev avadiislee pgmvkfprae vvhvgdrisa shfisarqad pastststst

stltpmptai ptpmpavasv tlpvaeqarh evfdvasvsa aaapvntlpv ttpqnlqtat

ygstlsgdnh srligsegst lsagedstli frlwdgkryr qlvartgeng veadipyyvn

5R5

edddivdkpd edddwievks skksgsysgs kgskrrilss kksgsysgsk gskrrnlssk

ksgsysgskg skrrilsskk sgsysgskgs krrnlsskks gsysgskgsk rril

Fig. S3 The amino acid sequences of recombinant protein INP-5R5. The sequences of INP and 5R5 are highlighted with blue and pink. A single repeating unit is underlined.

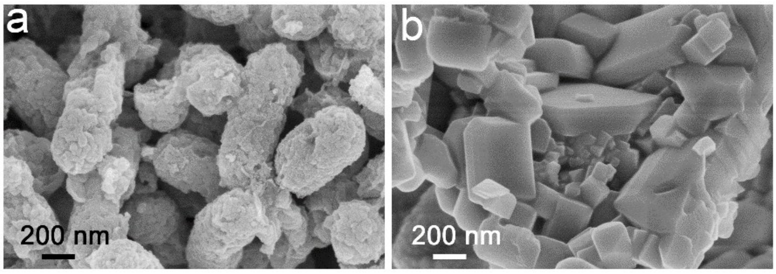

Fig. S4 SEM image of (a) 5-TiO_2 and (b) INP-modified product annealed under 600 °C in air.

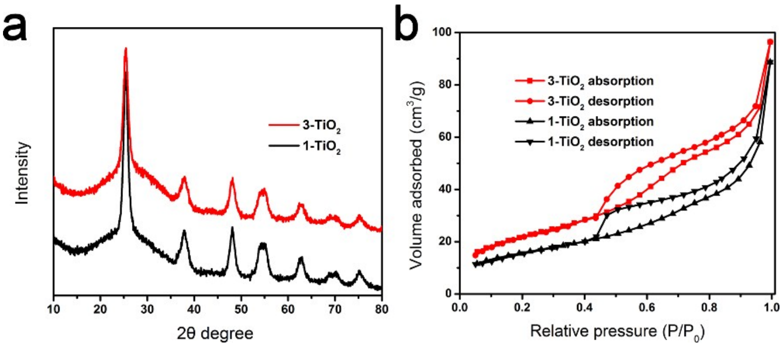

Fig. S5 (a) XRD patterns and (b) Nitrogen adsorption and desorption isotherms of 1-TiO_2 and 3-TiO_2.

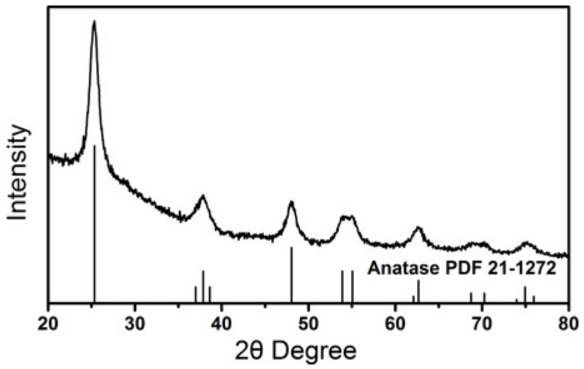

Fig. S6 XRD pattern of 5-TiO_2/C.

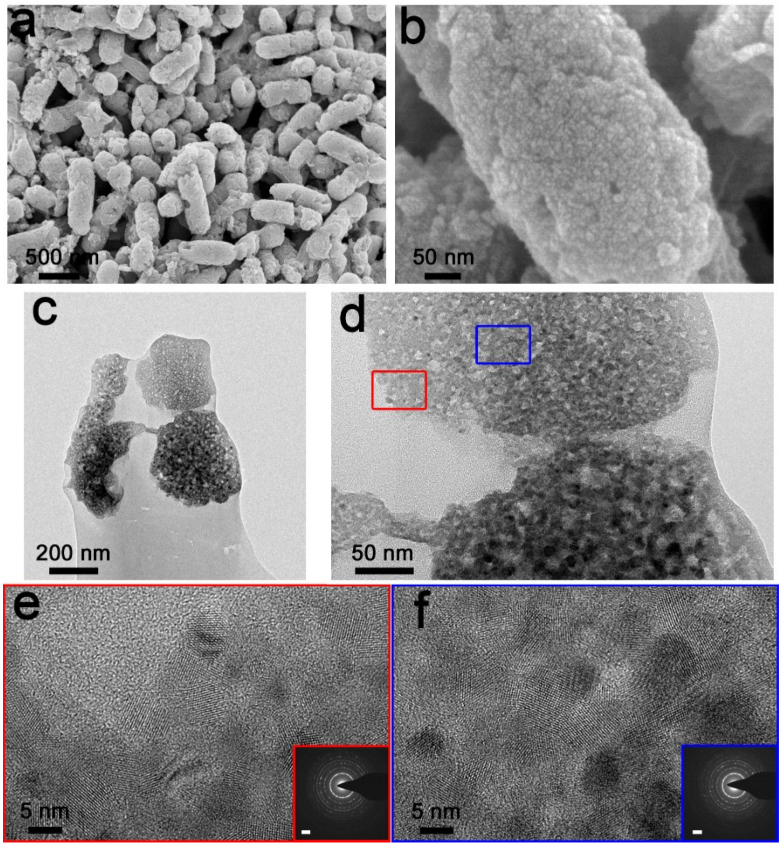

Fig. S7 (a) Low and (b) high magnification SEM images of 5-TiO_2/C. (c) Low and (d) high magnification TEM images of 5-TiO_2/C after treatment through ion beam milling. (e) and (f) high magnification TEM images and corresponding SAED (inset) of red and blue region in (d), respectively.

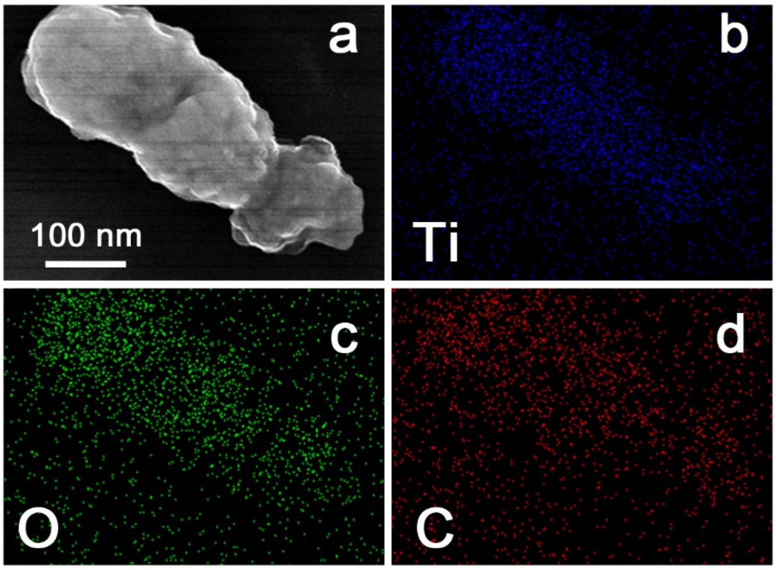

Fig. S8 (a) SEM image, (b) titanium, (c) oxygen, and (d) carbon element mapping images of as-prepared 5-TiO_2/C.

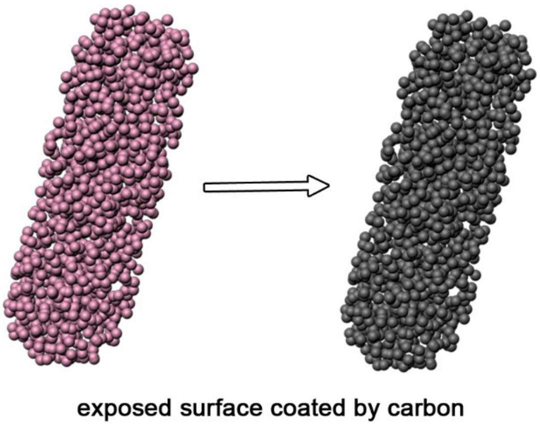

Fig. S9 Schematic diagram of the behavior of carbon coating. It is hypothesized that the exposed surface has been coated by carbon. The specific surface area of 5-TiO_2 is 87.8 m^2/g. The density of graphite carbon is 2.16 g/cm^3. The thickness of carbon layer is setting as 1 nm; the mass of a single anatase rod is setting as m. The surface area of a single anatase rod is 87.8*m. The volume of carbon layer is 87.8*m*1. The mass of carbon layer is 87.8*m*1*2.16. The carbon content is 15.8 wt%.

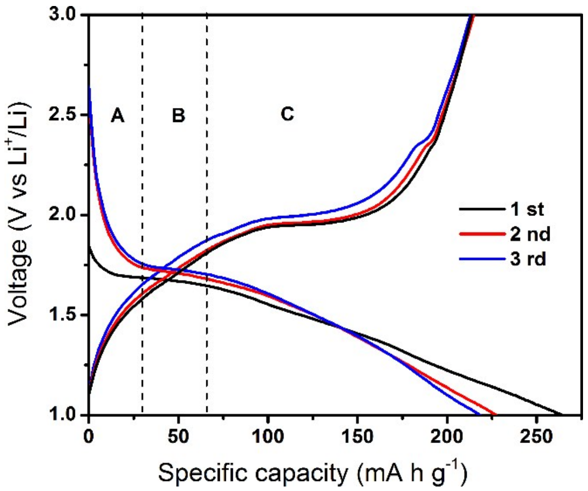

Fig. S10 Charge-discharge voltage profiles of the initial three cycles of 5-TiO_2/C electrode at a current rate of 1 C. There are three distinct regions of voltage change in the discharge profile. Region A displays a rapid drop from the open circuit potential to 1.75 V, which is considered as the homogenous Li^+ insertion into anatase. Region B is a two phase plateau at 1.75 V, known as the Li-rich phase coexisting with the Li-poor phase. Region C exhibits a gradually declining curve after the plateau region, which arises from the storage of Li^+ on the surface or interface of anatase nanoparticles.

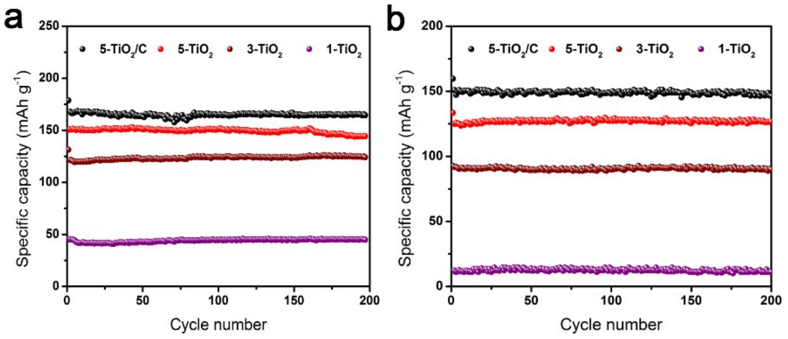

Fig. S11 Cycling performance of n-TiO_2 (n=1, 3, 5) and 5-TiO_2/C electrodes at a current rate of (a) 5 C and (b) 10 C.

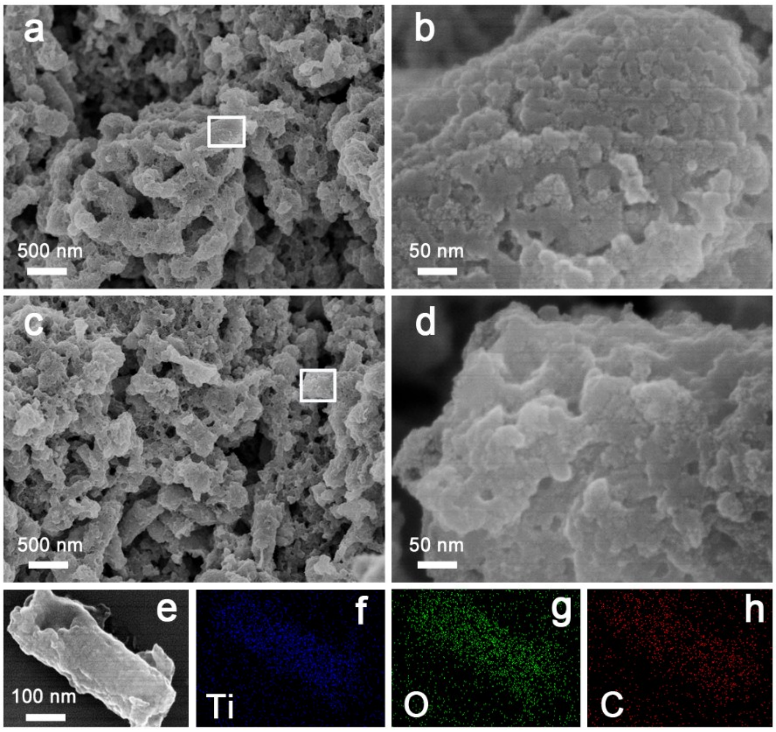

Fig. S12 The post-mortem characterization of 5-TiO_2 and 5-TiO_2/C electrodes after 200 charge-discharge cycles at current rate of 1 C. (a) Low and (b) high magnification SEM images of 5-TiO_2. (c) Low and (d) high magnification SEM images of 5-TiO_2/C. (e) SEM image, (f) titanium, (g) oxygen, and (h) carbon element mapping images of 5-TiO_2/C.

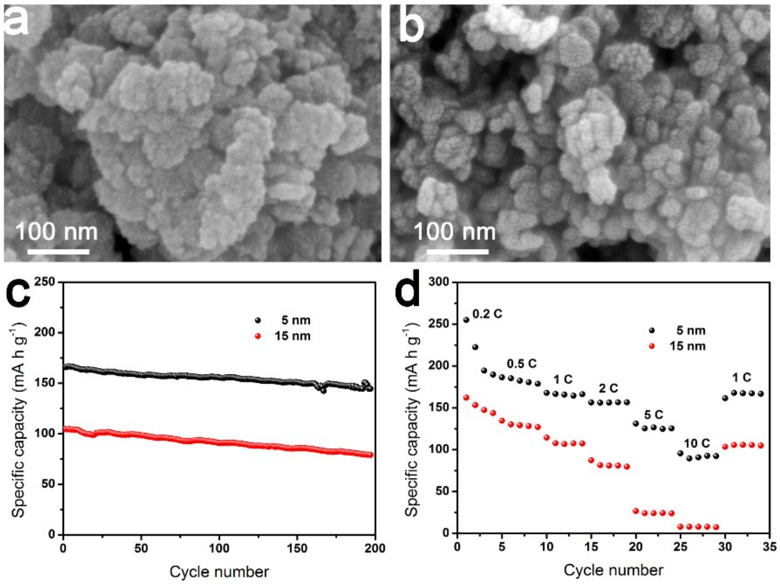

Fig. S13 SEM images of commercial anatase powder (a) 5 nm and (b) 15 nm. (c) Cycling performance at a current rate of 1 C. (d) Rate capability at various current rates.

Table S1. Comparison of electrochemical performance of various TiO_2 based materials.

Electrode materials	Specific capacity (mA h g^{-1})	Discharge rate (C) 1 C = 168 mA h g^{-1}	References
TiO_2-graphene hybrid	160	1 C	S1
	125	10 C	
TiO_2-graphene aerogels	200 (after 50 cycles)	0.59 C	S2
TiO_2 quantum dot-graphene nanosheet	190 (after 100 cycles)	1 C	S3
	145	10 C	
TiO_2 nanocrystals-RGO sheets	175	0.59 C	S4
	125	11.8 C	
TiO_2-graphene-TiO_2 sandwich-like nanosheets	237 (after 100 cycles)	0.1 C[a)]	S5
High aspect ratio TiO_2 nanotubes	~ 200	1 C	S6
	114 (after 6000 cycles)	30 C	
Mesoporous TiO_2 hollow spheres-graphitic carbon	175[b)]	1 C	S7
	137 (after 1000 cycles)	5 C	
TiO_2 hollow spheres	145.2	1 C[c)]	S8
	105.6	10 C	
TiO_2 mesocrystals	151.9	1 C	S9
TiO_2 nanosheets hierarchical spheres	174	1 C	S10
	150	10 C	
Multishelled TiO_2 hollow microspheres	237 (after 100 cycles)	1 C	S11
	119 (after 1200 cycles)	10 C	
Amorphous carbon coated TiO_2 nanocrystals	166 (after 100 cycles)	1 C	S12
Carbon coated TiO_2 nanorod	207 (after 200 cycles)	1 C	Our work
	149 (after 5000 cycles)	10 C	

[a)] 1 C = 200 mA h g^{-1},

[b)] voltage range 2.5 V-1.2 V,

[c)] 1 C = 173 mA h g^{-1}

Table S2. Kinetic parameters of 5-TiO_2 and 5-TiO_2/C electrodes. Rs, the ohmic resistance (including the electrolyte, separator, and electrical contacts resistance). Rct, the charge transfer resistance. W, the Warburg impedance of Li ion diffusion into the active materials.

	Rs (Ω)	Rct (Ω)	*W*
5-TiO_2	5.7	69.6	0.007
5-TiO_2/C	5.8	45.9	0.018

Supplementary References

S1. D. H. Wang, D. W. Choi, J. Li, Z. G. Yang, Z. M. Nie, R. Kou, D. H. Hu, C. M. Wang, L. V. Saraf, J. G. Zhang, I. A. Aksay and J. Liu, *ACS Nano*, 2009, **3**, 907-914.

S2. B. C. Qiu, M. Y. Xing and J. L. Zhang, *J. Am. Chem. Soc.,* 2014, **136**, 5852-5855.

S3. R. W. Mo, Z. Y. Lei, K. N. Sun and D. Rooney, *Adv. Mater.,* 2014, **26**, 2084-2088.

S4. W. Li, F. Wang, S. S. Feng, J. X. Wang, Z. K. Sun, B. Li, Y. H. Li, J. P. Yang, A. A. Elzatahry, Y. Y. Xia and D. Y. Zhao, *J. Am. Chem. Soc.,* 2013, **135**, 18300-18303.

S5. W. Li, F. Wang, Y. P. Liu, J. X. Wang, J. P. Yang, L. J. Zhang, A. A. Elzatahry, D. AlDahyan, Y. Y. Xia and D. Y. Zhao, *Nano Lett.,* 2015, **15**, 2186-2193.

S6. Y. X. Tang, Y. Y. Zhang, J. Y. Deng, D. P. Qi, W. R. Leow, J. Q. Wei, S. Y. Yin, Z. L.Dong, R. Yazami, Z. Chen, X. D. Chen, *Angew. Chem. Int. Edit.,* 2014, **53**, 13488-13492.

S7. H. Liu, W. Li, D. K. Shen, D. Y. Zhao, G. X. Wang, *J. Am. Chem. Soc.,* 2015, **137**, 13161-13166.

S8. G. Q. Zhang, H. B. Wu, T. Song, U. Paik, X. W. Lou, *Angew. Chem. Int. Edit.,* 2014, **53**, 12590-12593.

S9. J. F. Ye, W. Liu, J. G. Cai, S. A. Chen, X. W. Zhao, H. H. Zhou, L. M. Qi, *J. Am. Chem. Soc.,* 2011, **133**, 933-940.

S10. J. S. Chen, Y. L. Tan, C. M. Li, Y. L. Cheah, D. Y. Luan, S. Madhavi, F. Y. C. Boey, L. A. Archer, X. W. Lou, *J. Am. Chem. Soc.,* 2010, **132**, 6124-6130.

S11. H. Ren, R. B. Yu, J. Y. Wang, Q. Jin, M. Yang, D. Mao, D. Kisailus, H. J. Zhao, D. Wang, *Nano Lett.,* 2014, **14**, 6679-6684.

S12. T. Xia, W. Zhang, Z. H. Wang, Y. L. Zhang, X. Y. Song, J. Murowchick, V. Battaglia, G. Liu, X. B. Chen, *Nano Energy,* 2014, **6**, 109-118.